Suppressing sidechain modes and improving structural resolution for 2D IR spectroscopy via vibrational lifetimes

Kayla A. Hess, Cade K. Rohler, Lauren E. Buchanan*

Department of Chemistry, Vanderbilt University, 1234 Stevenson Center Lane, Nashville, Tennessee, United States

*Corresponding Author Email: lauren.e.buchanan@vanderbilt.edu

The following article has been submitted to the Journal of Chemical Physics.

ABSTRACT

Vibrational spectroscopy of protein structure often utilizes $^{13}C^{18}O$-labeling of backbone carbonyls to further increase structural resolution. Sidechains such as arginine, aspartate, and glutamate absorb within the same spectral region, however, complicating the analysis of isotope-labeled peaks. In this study, we report that the waiting time between pump and probe pulses in two-dimensional infrared spectroscopy can be used to suppress sidechain modes in favor of backbone amide I' modes based on differences in vibrational lifetimes. Further, differences in the lifetimes of $^{13}C^{18}O$-amide I' modes can aid assignment of secondary structure for labeled residues. Using model disordered and β-sheet peptides, it was determined that while β-sheets exhibit a longer lifetime than disordered structures, while amide I' modes in both secondary structures exhibit longer lifetimes than sidechain modes. Overall, this work demonstrates that collecting 2D IR data at delayed waiting times, based on differences in vibrational lifetime between modes, can be used to effectively suppress interfering sidechain modes and further identify secondary structures.

Keywords: 2D IR spectroscopy, vibrational lifetimes, sidechain absorption, isotope labeling

I. INTRODUCTION

Structure-dependent variations in the amide I' vibrational frequency allow infrared spectroscopy to serve as a powerful tool for protein characterization.[1,2] Changes in the amide I' frequency occur as a result of vibrational coupling between individual backbone amides. Couplings vary strongly between different structures, resulting in the amide I' mode of strongly coupled parallel β-sheets absorbing from ~1615 to 1630 cm^{-1},[3–6] while α-helices and disordered structures overlap heavily between ~1640 to 1660 cm^{-1}.[3,6,7] Ultrafast two-dimensional infrared (2D IR) spectroscopy provides additional information about peptide structure and dynamics that is not available via linear infrared techniques.[6,8,9] For example, analysis of 2D line shapes allows structural heterogeneity and environmental interactions to be determined,[8,10] while the presence of crosspeaks indicates the orientation and distance of different oscillators within a peptide.[6,8–10] The additional light-matter interactions present in 2D IR spectroscopy result in the signal strength scaling with transition dipole strength (μ) as $|\mu|^4$, compared to $|\mu|^2$ as in linear IR.[7] The resulting improvement in spectral resolution allows residue-specific structure to be observed through the incorporation of $^{13}C^{18}O$-isotope labels into the backbone carbonyl of a residue, which causes an ~55 cm^{-1} redshift in the amide I' frequency and spectrally isolates that residue from the rest of the protein.[3–5,11–14] Such labeling schemes have previously been utilized to monitor amyloid aggregation pathways,[3,4,15] identify structural differences in β-sheet-rich peptides,[5,11,12] and observe changes in α-helical structure.[7,13,16,17] While separated from the bulk amide I' backbone signal, the $^{13}C^{18}O$-labeled mode can overlap with amino acid sidechain modes,[7,18–20] with the most prominent being arginine (Arg, 1585-1610 cm^{-1}), aspartate (Asp, 1550-1590 cm^{-1}), and glutamate (Glu, 1550-1590 cm^{-1}).[9,18] Spectral crowding in proteins containing these residues complicates the assignment of $^{13}C^{18}O$-modes to specific secondary structures and requires the use of different strategies to remove interfering signals. Most often, researchers have turned to mutation, replacing IR-active sidechains with other residues. For example, this approach was used to examine the hydration of residues lining the transmembrane pore of the M2 proton channel of the influenza A virus, where two Asp residues were mutated to asparagine (Asn) to prevent overlap with $^{13}C^{18}O$-isotope signals.[19,20] However, such mutations can alter native protein structure and function; in the case of M2, Asn substitution increased the overall conduction of the channel, as well as the activation and conduction pK_a values.[19,20] A less perturbative approach would be isotope label IR-active sidechains in order to shift their vibrational frequencies away from the amide I' region.

While sidechain labeling has been demonstrated successfully in a limited number of studies,[21,22] this approach is often impractical as sidechain labels are typically more expensive and challenging to synthesize than backbone labels. Recent work in our group has shown that ratios of integrated peak areas can be used to make comparisons between multiple labeled and unlabeled variants of the same peptide to separate isotope signals from the sidechains, but this requires the use of multiple samples to make such comparisons.[7] Here, we demonstrate that differences in vibrational lifetimes between the sidechain and amide I' modes can be used to distinguish between the overlapping signals.

Traditionally, ultrafast pump-probe spectroscopy has been utilized to characterize vibrational lifetimes and population relaxation.[23,24] However, pump-probe spectra can suffer from spectral congestion, particularly for macromolecules such as proteins. Crosspeaks, which arise from vibrational coupling and energy transfer between modes, contribute to 1D spectra but are not easy to resolve and further complicate lifetime analysis (Fig. S1).[25] By instead utilizing 2D IR spectroscopy, which inherently has improved spectral resolution, and plotting the spectra over a second frequency dimension, which shifts the crosspeaks off the diagonal, better peak separation can be achieved.[26] Analogous to traditional pump-probe, the time delay between the second pump pulse and the probe pulse can be scanned in 2D IR spectroscopy to determine how the system evolves during the waiting time.[27] These waiting time studies provide additional information on molecular dynamics; for example, the formation of crosspeaks between different modes can be used to determine vibrational energy transfer during population relaxation.[24,26–28] Another common use of waiting studies is characterizing solvent exposure of residues within channel proteins and within amyloid fibrils.[19,20,29] Previous work by Middleton and coworkers characterized the impact of hydration on the lifetime of amide I' modes in human islet amyloid polypeptide (hIAPP).[27] The random coil and β-sheet modes were shown to have different vibrational lifetimes, with the disordered modes decaying more quickly as the waiting time was increased. Similar behavior was observed for $^{13}C^{18}O$-labeled residues with labels in less structured regions of the fibrils showing faster signal decay. For both the native and labeled modes, differences in lifetime were attributed to both increased structural disorder and higher solvent exposure for the disordered regions when compared to the β-sheets.[27] The ability to suppress the broad absorption of disordered structures via waiting times was noted as an important development that could allow further distinction between overlapping features, such as disordered and α-helical modes.[27] More recent work from

the Cho and Hunt groups varied waiting times to suppress signal from water to study protein dynamics in more native environments, such as blood serum, without the need for deuterated solvents.[30–32] The differences in lifetimes between $\delta_{H\text{-}O\text{-}H}$ water mode and amide I mode, as well as the signal enhancement provided by $|\mu|^4$ scaling in 2D IR, allows the amide signal to dominate when 2D IR spectra were collected with a 250 fs delay between the pump and probe pulses.[30,31]

In this work, we demonstrate that the waiting time delay in 2D IR spectroscopy can also be used to suppress sidechain features and reveal underlying isotope-labeled amide I' modes. Using two model peptides, we determine differences in vibrational lifetimes between vibrational modes arising from amino acid sidechains and both native and $^{13}C^{18}O$-labeled backbone carbonyls. First, we demonstrate the suppression of a strong Asp mode that fully obscures the $^{13}C^{18}O$-labeled amide mode in a model α-helical peptide (MAHP, DPAEAAKAAAGR-NH_2) that we have studied previously.[7] In that work, MAHP was shown to be primarily disordered at low pH and partially helical at high pH, with high helicity only being achieved after the introduction of a trifluoroethanol cosolvent. As the pH was increased, however, a strong Asp mode appeared at ~1580 cm^{-1}, overlapping heavily with isotope-labeled modes.[7] For this study, we focus on the suppression of the Asp mode via 2D IR waiting times. Changes in solvent polarity are known to affect vibrational lifetimes,[26,28] so no cosolvents are added to increase helicity, leaving MAHP in a partially disordered state. However, the acronym MAHP is still used for consistency between the studies. Two isotope-labeled variants are utilized in this study, one with a single label at alanine-5 (A5) and one with double labels at alanine-5 and alanine-8 (A5A8). We demonstrate that the $^{13}C^{18}O$ amide I' peak in A5A8 has a longer lifetime than in A5, which we attribute to coupling between the paired labels that is not present in the singly labeled peptide.[7] Both the coupled and uncoupled isotope labels exhibit a longer lifetime than the Asp sidechain modes, however, enabling waiting times to be used to suppress unwanted sidechain features while retaining labeled amide I' modes needed to resolve structure at the residue level. Second, we use human islet amyloid polypeptide (hIAPP), an amyloidogenic peptide associated with type II diabetes, as a model β-sheet. Again, two isotope-labeled variants are studied: valine-17 (V17), which participates in the extended β-sheet structure of hIAPP fibrils, and phenylalanine-23 (F23), which remains disordered within the fibrils. Again, we observe clear suppression of overlapping sidechain modes, in this case Arg. Further, labels within more ordered β-sheets display longer lifetimes than those found in

partially helical or disordered structures, allowing us to distinguish secondary structure for individual residues.

II. MATERIALS AND METHODS

Materials

All reagents were used as purchased, with the exception of modifications made to 1-^{13}C-alanine, 1-^{13}C-phenylalanine, and 1-^{13}C-valine described in detail in the preparation of Fmoc-$^{13}C^{18}O$-labled amino acids. Acetic anhydride, acetone, acetonitrile, diethyl ether, dimethylformamide (DMF), hydrochloric acid (HCl, 12.1 N), methanol, 4-nitrobenzyaldehyde (4NBA), potassium bisulfate ($KHSO_4$), and sodium bicarbonate ($NaHCO_3$) were purchased from Fisher Scientific (Pittsburg, PA, USA). Anisole, thioanisole, 1,2-ethanedithiol, and sodium deuteroxide (NaOD, 30 wt. %) were purchased from Acros Organics (Geel, Antwerp, Belgium). Oxyma, Rink Amide ProTide resins, and Fmoc-protected amino acids were purchased from CEM (Matthews, NC, USA). N-(9-Fluorenylmethoxycarbonyloxy)succinimide (Fmoc-Osu), N-methyl-2-pyrrolidinone, and N,N'-diisopropylcarbodiimide, were purchased from Oakwood Chemical (Estill, SC, USA). 1-^{13}C-L-alanine (99% enriched), 1-^{13}C-L-phenylalanine (99% enriched), and 1-^{13}C-L-valine (99% enriched) and ^{18}O-H_2O (98% enriched) were purchased from Cambridge Isotope Laboratories (Tewksbury, MA, USA). N-methylacetamide (NMA) and piperazine were purchased from Alfa Aesar (Ward Hill, MA, USA). All other reagents were purchased from Millipore Sigma (Burlington, MA, USA).

Preparation of Fmoc-$^{13}C^{18}O$ -labeled amino acids

Detailed methods for $^{13}C^{18}O^{18}O$ isotope labeling have been previously published.[14,15] Fmoc-protection of commercial ^{13}C-labeled amino acids was achieved using a 1:1:1 ratio of the amino acid, Fmoc-Osu, and $NaHCO_3$ in a 50:50 water:acetone mixture. The mixture was stirred at room temperature for 24 hours, then quenched using 2 M $KHSO_4$ to lower the pH to 2 and precipitate the product. The precipitate was vacuum filtered and washed with ice-cold water to remove any salt. Four washes were performed, and the product was lyophilized between washes to remove any excess water. Subsequently, an acid-catalyzed ^{18}O-isotope exchange was utilized to produce $^{13}C^{18}O^{18}O$-labeled amino acids. These reactions were performed by dissolving 1 g Fmoc-^{13}C-amino acid and 1 g $^{18}OH_2$ in 8 mL dioxane and 4 mL 4 M HCl in dioxane and refluxed under inert

conditions at 150 °C for four hours. The reaction mixture was lyophilized to isolate the product. The reaction was performed two additional times to achieve greater than 90% labeling efficiency, as confirmed via electrospray ionization mass spectroscopy (ESI-MS, Orbitrap XL Penn, Thermofisher, WA, USA). The final product was purified by diethyl ether extraction to remove any remaining salt.[15]

Peptide synthesis and purification

Detailed methods for synthesis and cleavage of hIAPP[15] and MAHP[7] have been described previously and were performed with slight modifications to the MAHP cleavage protocol and the hIAPP purification method. Briefly, both peptides were synthesized with a Liberty Blue microwave peptide synthesizer (CEM, Matthews, NC, USA) using standard Fmoc solid-phase peptide synthesis (SPPS) with Rink Amide ProTide resin to produce an amidated C-terminus for both peptides and pseudoprolines to prevent aggregation for hIAPP.[33] A cleavage cocktail of 90% trifluoroacetic acid, 5% 1,2-ethanedithiol, 2.5% anisole, and 2.5% thioanisole was used to cleave the peptides from the resin. After stirring at room temperature for 2.5 hours, the mixture was filtered directly into ice-cold diethyl ether to remove the resin and precipitate the peptides. The peptides were centrifuged at 5000 rpm for five minutes and the supernatant decanted to remove remaining organics. The washing process was repeated two additional times with fresh diethyl ether. Prior to purification, the solubility of hIAPP was increased by dissolving it in 20% acetic acid (5 mg/mL) and then lyophilizing to remove the solvent.[33] The peptide was dissolved in dimethyl sulfoxide (DMSO) at 2.5 mg/mL and allowed to sit at room temperature for 48 hours to promote a disulfide bond between Cys2 and Cys7. Finally, hIAPP was diluted to 1.25 mg/mL using water. MAHP was dissolved in water at 2 mg/mL. Both peptides were purified using reverse phase high-performance liquid chromatography (HPLC, Ultimate 3000, ThermoFisher, Waltham, MA, USA). A binary gradient was utilized, with 100% water with 0.045% HCl (solvent A) and 90% acetonitrile with 10% water and 0.045% HCl (solvent B). For hIAPP, the gradient was varied from 30 to 45% B over the course of 15 minutes while UV absorbance was monitored at 215 and 280 nm; hIAPP eluted at approximately 11 minutes. For MAHP, the gradient was varied from 0 to 40% B over the course of 20 minutes while UV absorbance was monitored at 215 nm; MAHP eluted at approximately 11 minutes. The purified peptides were characterized using ESI-MS. Isotope labeled peptides (single-labeled V17 and F23 hIAPP, single-labeled A5 MAHP, and double-labeled

A5A8 MAHP) were prepared in the same manner, but with the appropriate $^{13}C^{18}O^{18}O$ amino acids substituted within the synthesis protocol.

2D IR Sample preparation

Approximately 1 mM stocks of hIAPP were prepared in deuterated 1,1,1,3,3,3-hexafluoro-2-propanol (dHFIP). The stock solutions were sonicated then allowed to sit at room temperature overnight to fully disaggregate the fibrils. Stock solutions of MAHP were prepared in D_2O at approximately 10 mM. Precise concentrations were determined using a NanoDrop One^C Micro-UV/Visible spectrophotometer (Thermo Fisher Scientific, Wilmington, DE, USA). Individual samples of hIAPP were prepared for 2D IR by lyophilizing an aliquot of stock solution and dissolved in 20 mM deuterated Tris buffer (pH ~7.6) at a final concentration of 1 mM. Individual samples of MAHP were prepared for 2D IR by diluting to 5 mM in D_2O. Due to purification conditions, MAHP in D_2O is typically acidic (pH 3), which was confirmed prior to all 2D IR experiments. For high pH samples, NaOD was used to adjust to pH 10. For validation studies, 120 mM NMA was prepared in D_2O. Samples were deposited between two CaF_2 windows (Crystan, Poole, Dorset, UK) with 50 μm Teflon spacers. Each hIAPP sample was allowed to aggregate for a minimum of 2 hours to ensure the formation of amyloid fibrils.

2D IR measurements

Comprehensive methods for 2D IR data collection and processing have been described previously.[11,14] 800 nm pulses (7 W, 1 kHz, 60 fs) were generated using a single box ultrafast amplifier (Solstice, SpectraPhysics, Milpitas, CA, USA). Half of the output was used to generate mid-IR light (6150 nm, 25 mW, 1 kHz, <100 fs) via an optical parametric amplifier with difference frequency generation (TOPAS-Prime, SpectraPhysics, Milpitas, CA, USA). The mid-IR beam was steered into a 2D IR spectrometer (2DQuick IR, PhaseTech Spectroscopy, Madison, WI, USA) and split into pump and probe beams. The polarization of the pump beam was rotated by the magic angle (54.7°) relative to the probe in order to eliminate rotational contributions to the 2D IR spectral dynamics. The signal was dispersed by a monochromator (Princeton Instruments, Trinton, NJ, USA) onto a mercury cadmium telluride focal-plane array detector (PhaseTech Spectroscopy, Madison, WI, USA). The delay time between pump and probe pulses (T_2) was varied from 0 to 4363 fs, with the step size increasing exponentially from 200 fs. PhaseTech QuickControl software was used to collect data and all data was processed using custom MATLAB scripts. 4NBA was

utilized as a calibration standard. For hIAPP, 10 scans were taken at each delay time. For MAHP, a minimum of 10 scans were taken at early delay times and the number of scans was increased to a minimum of 25 scans for delay times greater than 2000 fs. Three replicates were taken for each sample. To determine the lifetimes using 2D IR spectra, the diagonal was set through the center of the fundamental (v=0→1) peak for the 0 fs delay and the highest intensity frequency was selected. The intensity at this frequency was obtained for all subsequent delay times and plotted as a function of waiting time, T_2 (Fig. S2). The data for each replicate was fit to a biexponential decay, comprising time constants τ_1 and τ_2 and corresponding amplitudes a_1 and a_2, with a constant baseline offset (y_0), as shown in Equation 1.[23,28]

$$A = y_0 + a_1 e^{-T_2/\tau_1} + a_2 e^{-T_2/\tau_2} \quad (1)$$

III. RESULTS AND DISCUSSION

The first peptide studied was MAHP. In a previous study, we showed that MAHP can shift from a disordered structure to a partially α-helical structure as pH is increased from pH 3-10.[7] At pH 3, unlabeled MAHP (UL MAHP) displays a pair of peaks at ~1650 cm^{-1}, corresponding to a primarily disordered structure. A slight redshift to 1645 cm^{-1} is observed at pH 10, which can be attributed to the formation of a partial α-helix (~1 turn) (Fig. 1A and Fig. S3A). Greater helicity can be achieved through the addition of a cosolvent such as 2,2,2-trifluoroethanol,[7] but changing solvent composition can impact the lifetime of amide I' modes.[28] Thus, no cosolvent was used in this study to enable direct comparison between samples.

While MAHP is mostly disordered at both low and high pH, increasing the pH dramatically impacts the appearance of sidechain peaks. MAHP contains three IR active sidechain modes: Arg, Asp, and Glu. At low pH, an Arg $C{=}NH_2$ mode appears between 1600 to 1610 cm^{-1} (Fig. S3A). This mode would overlap with ^{13}C-labeled modes, if they were being used, but does not interfere with the $^{13}C^{18}O$ modes that are of interest in this study, regardless of the pH conditions. However, as pH is increased to induce changes in the secondary structure, the deprotonation of Asp and Glu sidechains generates a peak at 1560 to 1590 cm^{-1} (Fig. 1A), which overlaps the spectral window over which $^{13}C^{18}O$-labeled amide I' peaks appear. This can be seen by comparing spectra of UL MAHP at pH 10 (Fig. 1A) to spectra of MAHP at pH 3 with labels at A5 (Fig. 1D) and A5A8 (Fig.

1G). For both A5 and A5A8 at low pH, peaks corresponding solely to the $^{13}C^{18}O$-labels occur between 1580-1585 cm^{-1}. The single $^{13}C^{18}O$-backbone label in A5 differs in energy from the UL backbone modes sufficiently enough that it does not experience vibrational coupling. However, the paired labels in A5A8 allow for coupling between those two residues. Our previous study showed that MAHP forms a helical turn between these residues first when folding, so some weak coupling between the modes is expected due to transient helices even in the primarily disordered low pH condition.[7] The use of dual labels and the effects of vibrational delocalization due to coupling lead to A5A8 consistently exhibiting a more intense isotope peak than A5. Yet, at high pH conditions and a 0 fs T_2 delay, the Asp/Glu sidechain peaks are more intense than the isotope labeled peaks in either A5 or A5A8.

When T_2 is set to 426 fs, crosspeaks between the sidechain and UL backbones become more distinct at both low and high pH (Fig. 1B). At low pH, crosspeaks are observed between the UL backbone mode and the higher frequency Arg mode (Fig. S3B) and persist as the waiting time is increased to 681.4 fs, although the overall signal to noise ratio decreases at longer waiting times (Fig. S3C). At high pH, a new set of crosspeaks between the lower frequency Asp/Glu modes and the UL backbone also becomes apparent (Fig. 1B). The formation and evolution of crosspeaks as a function of waiting time has previously been observed for a small labeled peptide, where crosspeak intensity increased as the waiting time increased due to vibrational energy transfer between coupled modes.[24] The UL MAHP spectra suggest that the UL backbone amide I' modes are coupled to both the higher frequency Arg modes as well as the lower frequency Asp and Glu modes, depending on the pH. However, as the waiting times increase from 426 fs to 681.4 fs for UL MAHP at high pH, the lower frequency sidechain diagonal peaks as their corresponding crosspeaks weaken considerably compared to the UL amide I' diagonal peaks (Fig. 1B,C). Similarly, for UL MAHP at low pH the diagonal peaks resulting from Arg are largely gone by 681.4 fs, but the crosspeak with the backbone remains, suggesting that there is continued vibrational energy transfer between the modes.

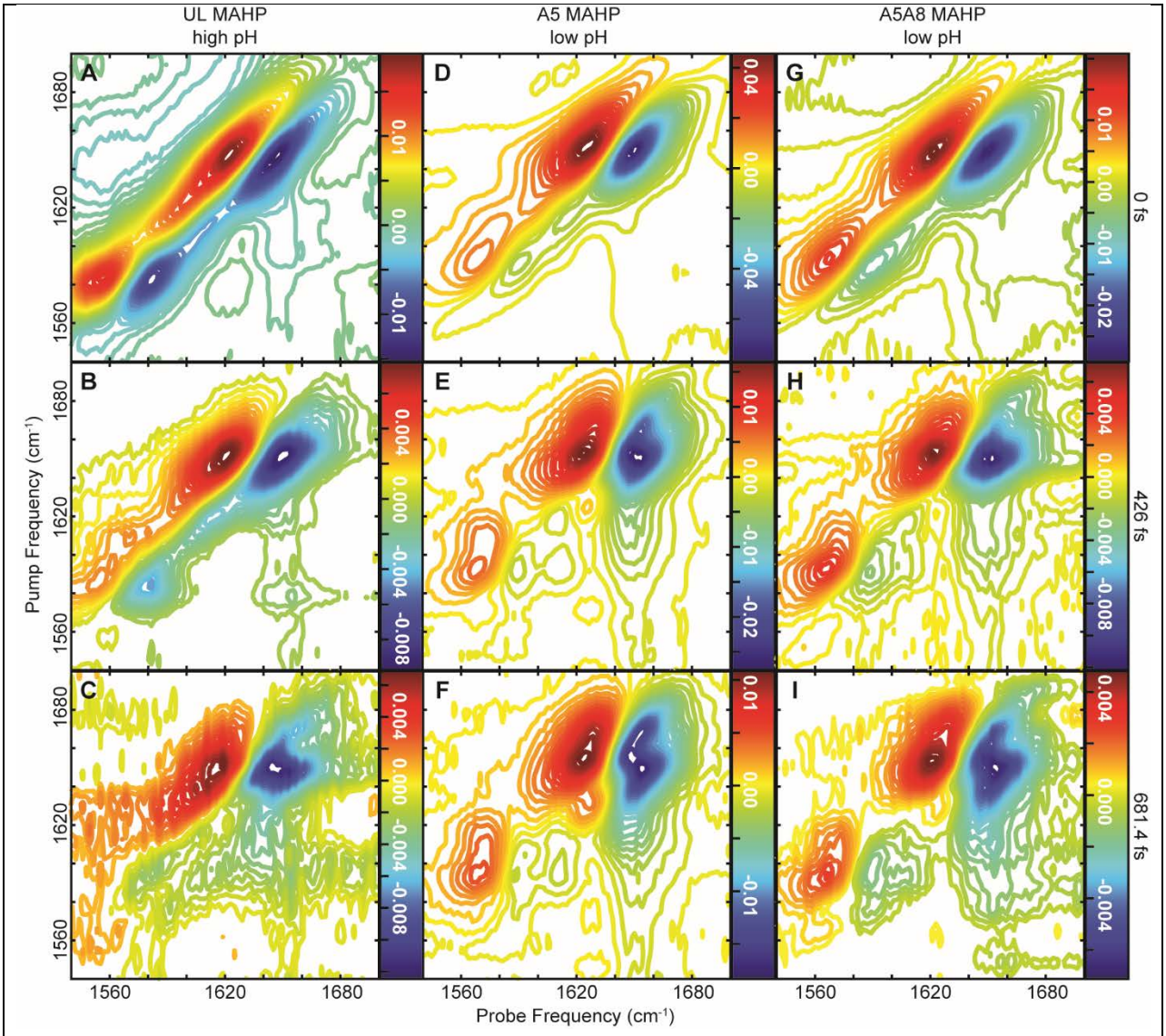

Figure 1: 2D IR spectra of (A-C) UL MAHP at high pH, (D-F) A5 MAHP at low pH, and (G-I) A5A8 MAHP at low pH with waiting times of 0, 426, and 681.4 fs, demonstrating the differences in signal between sidechain and $^{13}C^{18}O$-label modes.

For the isotope-labeled A5 and A5A8 samples at low pH (Fig. 1E,H), crosspeaks begin to form between the UL backbone and both the Arg and $^{13}C^{18}O$ modes as waiting time increases. The isotope peak for A5 also begins to form a crosspeak with the Arg mode (Fig. 1E,F), potentially indicating vibrational energy transfer between the Arg sidechain modes and $^{13}C^{18}O$ mode. There appears to be the beginning of the formation of a crosspeak between the Arg and $^{13}C^{18}O$ modes for the A5A8 isotope peak (Fig. 1H,I), but it is less pronounced than A5. For the isotope-labeled A5 and A5A8 samples at high pH, the isotope label peaks overlap significantly with the Asp/Glu

sidechain modes (Fig. S3E,F,H,I). However, signal in this region persists longer in the labeled samples than in UL MAHP at high pH, clearly visible even at 681.4 fs. We attribute this longer-lived signal to the $^{13}C^{18}O$-labeled amide I' modes, which suggests that there is an inherent difference in vibrational lifetime between modes arising from proteins backbone versus sidechains.

To further quantify the differences in lifetimes for the sidechain and backbone modes, additional 2D IR spectra of each sample were collected at waiting times ranging from 0 to 4363 fs. Frequencies were selected based on the diagonal trace from waiting time 0 fs for each peptide and the intensity at that frequency versus waiting time was fit to Equation 1. Once fit, there is a clear qualitative difference between the normalized decay curves (Fig. 2). The rapid decay of the sidechain signal (green) can be seen within the first 200 fs. The unlabeled backbone (blue) and doubly labeled A5A8 backbone (purple) signals decay more slowly, while the decay of the singly labeled A5 backbone (orange) signal falls somewhere in the middle. The region highlighted in gray indicates waiting times during which the sidechain signal has almost fully decayed, but both native and $^{13}C^{18}O$-labeled amide I' signals remain. This supports our observations in the 2D IR spectra obtained at 681.4 fs (Fig. 1C,F,I), where the peaks arising from isotope modes are still clearly distinguishable while the sidechain modes have become indistinguishable from the background noise. By collecting 2D IR spectra at waiting times within the shaded region, isotope labels can easily be differentiated from overlapping sidechains and analyzed without the need for sidechain mutation, although proper quantification of the relative vibrational lifetimes can help establish the optimal time delay.

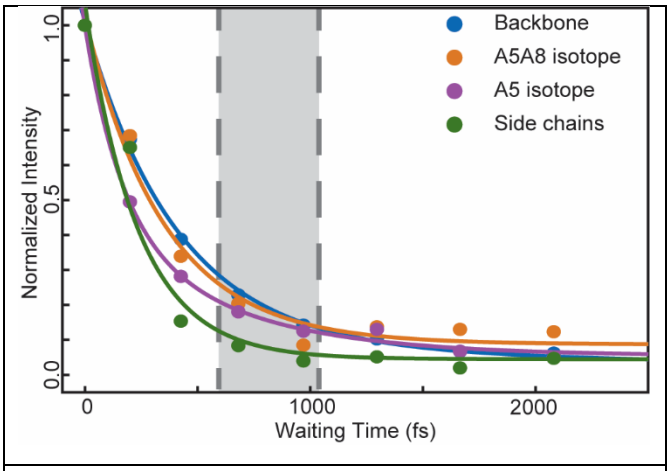

Figure 2: Representative traces of intensity versus waiting time for UL MAHP backbone (blue), A5A8 isotope label (orange), A5 isotope label (purple), and sidechain (green) modes. Experimental data (filled circles) was fit to a biexponential decay (Eq. 1, lines) and normalized to highlight the faster decay of the sidechain signal compared to isotope signal. The grey box indicates the waiting time period during which sidechain signal approaches zero, but isotope label signal persists.

The vibrational decay for each peptide was fit to a biexponential decay (Eq. 1) comprising a fast component (τ_1) on the time scale of 200-500 fs and slow component (τ_2) of 0.5-1.9 ps. For comparison, we also fit waiting time data extracted from 2D IR spectra of NMA, a common model of a single, localized amide bond. The biexponential fit yielded a τ_1 of 247 ± 12 fs and a τ_2 of 1743 ± 401 fs, which agree with the literature.[23,26,28] Similarly, the values obtained for both native and labeled amide I' modes agree with results by Hamm and coworkers, who studied peptides with a variety of secondary structures.[23] They attributed the slow component to vibrational population relaxation and the fast component to the dephasing of the initial vibrational state following excitation by the pump.[23] Pure dephasing is often attributed to changes in the environment.[9] In this work, variations between different secondary structures were seen in both lifetime components, suggesting that dephasing and population relaxation differ between the modes studied. Notably, while all backbone modes exhibited a τ_2 value of 1.0 ps or higher, the Asp/Glu sidechain modes displayed a much shorter second component of 449 ± 36 fs. However, for each mode studied, the faster component contributed more strongly to the overall fit, as indicated by their relative amplitudes, suggesting that τ_1 dominates the 2D IR signal decay. For this reason, our discussion will focus on τ_1(Table 1) as route towards distinguishing and suppressing side chain modes while maintaining useful 2D IR signal, although all fitting parameters are summarized in Table S1.

Table 1: τ_1 fit parameters for magic angle 2D IR measurements

	Conditions	τ_1 (fs)
NMA		247 ± 12
MAHP backbone	High/low pH	375 ± 19
Asp/Glu sidechains	High pH	206 ± 8
A5A8 labels	Low pH	324 ± 5
A5 label	Low pH	275 ± 3
hIAPP backbone		500 ± 25
V17 label		343 ± 12

The unlabeled backbone mode of MAHP was analyzed at both low and high pH conditions. pH was found to have a negligible impact on the lifetime of the unlabeled amide I' backbone mode of MAHP as the peptide remained primarily disordered at both conditions, yielding an average lifetime of 375 ± 19 fs across both conditions. The introduction of isotope labels also did not impact the lifetime of the unlabeled amide I' mode. To isolate the lifetimes of the $^{13}C^{18}O$-labels from the overlapping Asp and Glu modes at high pH, the lifetimes of A5 and A5A8 isotope modes at low pH were compared to UL MAHP sidechain modes at high pH. The single $^{13}C^{18}O$-isotope in A5 displays a lifetime of 275 ± 3 fs, while the double labels in A5A8 have a longer lifetime 324 ± 5 fs. At high pH, the Asp and

Glu peaks exhibit a lifetime of 206 ± 8 fs, which is much shorter than the lifetimes of both the UL and labeled amide I' backbone modes. Previous studies have attributed differences in amide I' lifetime to solvation effects, with the backbone modes of solvent exposed residues exhibiting shorter lifetimes.[27] Additionally, different vibrational modes inherently display unique vibrational lifetimes; novel vibrational probes often introduce heavy atoms that interrupt intramolecular relaxation pathways in order to extend vibrational lifetimes and study longer timescale dynamics.[34–38] Changes in solvation and mass could both contribute to the observed differences in the lifetimes between the sidechain and backbone modes. However, there are also differences in the $\tau_1$components for the UL, A5, and A5A8 amide I' modes that cannot be explained simply by differences in solvation or chemical bonding. Due to the mostly disordered structure of MAHP, all backbone amides should experience a similar degree of solvation, resulting in similar lifetimes for the UL and labeled modes. One possibility is that the differences in τ_1 must arise from small differences in vibrational coupling. The single label in A5 is unable to effectively couple with any unlabeled amide I' modes due to the energy difference, resulting in its $^{13}C^{18}O$ mode having shortest lifetime of any backbone mode. As previously discussed, there is likely at least a small amount of transient helical structures at low pH that allows for coupling between the different backbone modes. Thus, the paired isotope labels in A5A8 may experience weak coupling due to partial helix formation at the center of the peptide sequence. The UL backbone mode, however, exhibits the longest lifetimes as the many identical unlabeled amide I' modes can experience nearest neighbor couplings between adjacent residues, even in disordered structures.[39]

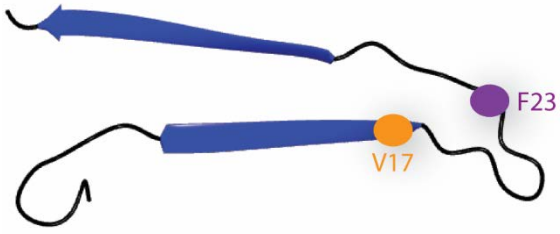

Figure 3: Structural modal of hIAPP fibrils derived from ssNMR,[40] with residues V17 and F23 highlighted in orange and purple, respectively.

To further examine the influence of coupling and secondary structure on lifetimes, hIAPP was utilized as a model β-sheet peptide due to its propensity to form well-ordered amyloid fibrils that should experience a high degree of coupling.[40] Middleton and coworkers previously collected 2D IR spectra of hIAPP at waiting times of 0, 500, and 1000 fs and compared the relative change in intensity for peaks representing different regions of secondary structure.[27] They concluded that increased hydration of disordered regions led to shorter amide I' lifetimes, while more ordered, and thus solvent-

protected, residues have longer lifetimes. Here, we isotope labeled two residues within hIAPP (Fig. 3) to quantify their vibrational lifetimes relative to overlapping sidechain modes. hIAPP aggregates always exhibit a strong peak pair at ~1620 cm^{-1}, which arise from highly ordered, extended β-sheets within the amyloid fibrils (Fig. 4). Due to the presence of the disordered N-terminus and partially disordered loop structure, some absorption remains within the disordered region at ~1650 cm^{-1} in each peptide. For UL hIAPP, there is a small shoulder to the red of the β-sheet peak, centered at ~1595 (Fig 4A). As UL hIAPP has no $^{13}C^{18}O$ label, we attribute this shoulder to the $C{=}NH_2$ mode from Arg sidechains.[18] Of the two labeled residues, F23 falls within a partially disordered loop in hIAPP fibrils while V17 falls within a highly ordered β-strand (Fig. 3). Thus, their amide I' modes should experience different coupling based on their positions within the fibril, with V17 being more strongly coupled than F23. At a waiting time of 0 fs, the F23 $^{13}C^{18}O$-amide I' backbone mode appears as a weak shoulder at 1593 cm^{-1} (Fig. 4D), indicating minimal coupling to other residues. Due to significant overlap with the Arg mode, spectra from V17 and UL hIAPP are nearly identical at 0 fs. The V17 mode is red-shifted to 1583 cm^{-1} due to stronger coupling within the β-sheet and is well separated from the Arg sidechain mode, although it would overlap with the signatures from Asp/Glu, as observed in MAHP, if they were present.

As the waiting time is increased, crosspeaks begin to form between the β-sheet and disordered peaks within UL hIAPP (Fig. 4B), indicating energy transfer between the amide I' modes arising from each structural region. The low-frequency shoulder due to the Arg sidechain decreases in intensity by 426 fs, but crosspeaks with the UL β-sheet peak become more apparent (Fig. 4B). By 970 fs, the Arg sidechain peaks are no longer visible, but its well-defined crosspeaks persist (Fig. 4C). The disappearance of sidechain modes with persistent crosspeaks matches behavior observed in UL MAHP, but occurs at a longer waiting time, likely due to the increased lifetime of β-sheet structures, which will be further discussed below. As the waiting time is increased to 426 fs, the F23 peak becomes more apparent (Fig. 4E), with greater intensity remaining around 1593 cm^{-1} than observed for the Arg peak in UL hIAPP at the same waiting time. Much like the A5 label in MAHP, F23 appears to have a slightly longer lifetime than the sidechain mode despite being existing in a disordered region of the peptide backbone, likely due to inherent differences in lifetime between amide I' modes and $C{=}NH_2$ modes. By 970 fs, the F23 peak is no longer visible (Fig. 4F). The intensity of the V17 isotope peak decreases more slowly as waiting time increases,

with the peak pair is still clearly visible at both 426 fs (Fig. 4H) and 970 fs (Fig. 4I), suggestion it has a longer lifetime than either the uncoupled F23 label or the Arg sidechain.

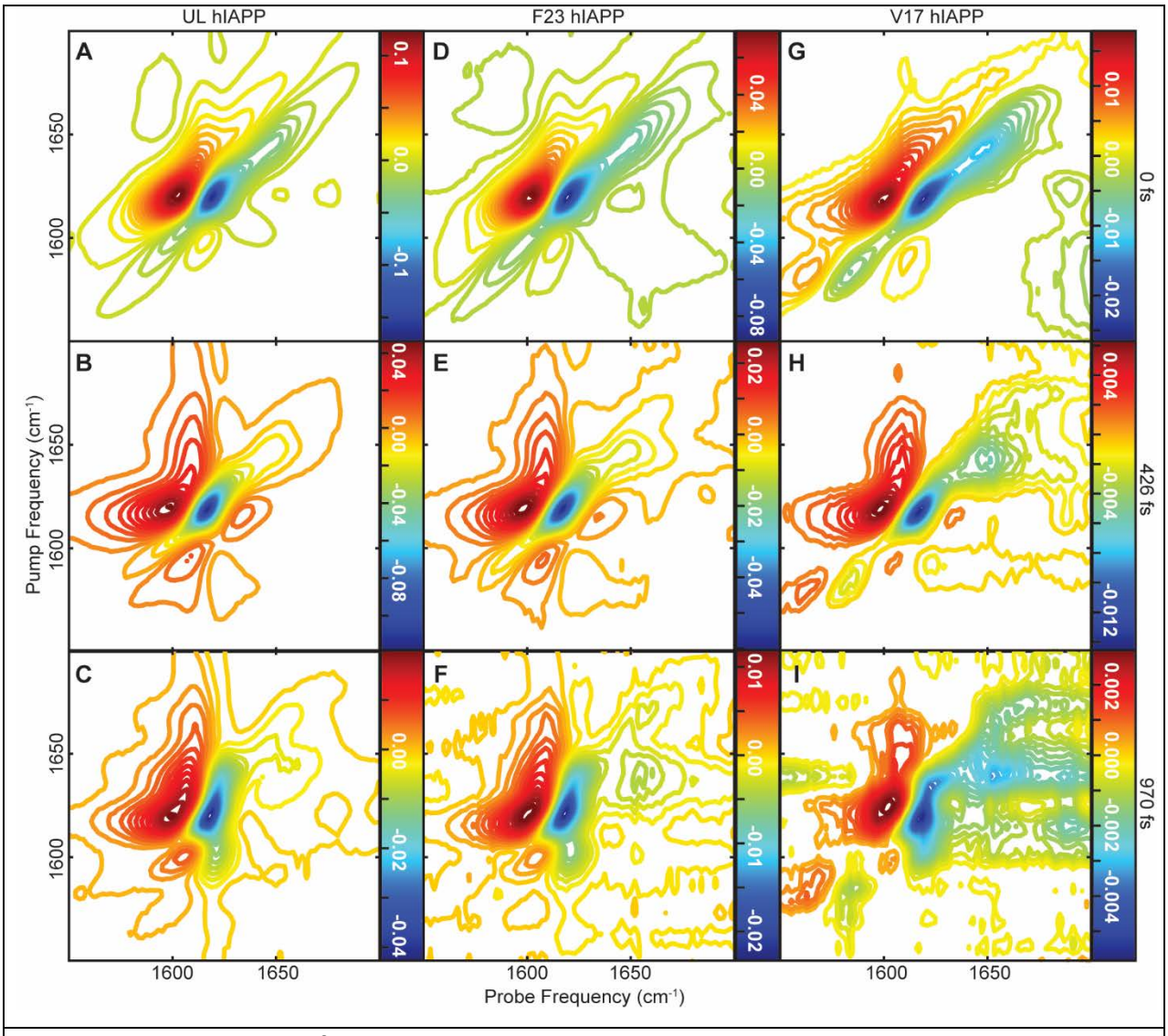

Figure 4: 2D IR spectra of (A-C) UL hIAPP, (D-F) F23 hIAPP, and (G-I) V17 hIAPP with waiting times of 0, 426, and 970 fs.

To quantify the differences in lifetime, the time dependence of the hIAPP UL β-sheet and V17 isotope peak intensities were fit to the same biexponential decay (Eq. 1) as used for MAHP. As with MAHP, we will focus on the faster decay component (Table 1) as it has a larger impact on the 2D IR signals observed. Example fits and all fit parameters are shown in Fig. S4 and Table S1, respectively. The unlabeled β-sheet mode displayed a lifetime of 500 ± 25 fs, while the V17 isotope label displayed a lifetime of 343 ± 12 fs. The highly coupled and ordered nature of the β-sheets, as

well as reduced hydration, likely contribute to the longer lifetime of the UL backbone mode in hIAPP compared to MAHP. Like MAHP, the V17 isotope label displayed a shorter lifetime than the bulk peptide; however, the V17 label does have a slightly longer lifetime than either the A5 or A5A8 labeled modes, most likely due to its more ordered secondary structure. Unfortunately, the F23 peak could not be isolated effectively from the Arg sidechain peak, and interference from the overlapping crosspeak between the UL backbone and Arg modes that grew in at longer delays further complicated attempts at fitting the time-dependence of F23 signals. Instead, the decrease in signal intensity at 426 fs relative to 0 fs can be used to compare the V17 and F23 isotopes. In the F23 sample, the 1595 cm^{-1} intensity decreased to 21% of the original intensity, while a decrease of 11% was observed at the same frequency in the UL hIAPP sample. As UL hIAPP only has contributions from the Arg sidechains in this region while F23 hIAPP has contributions from both the labeled amide I' and the Arg modes the longer-lived signal in F23 can thus be attributed to the isotope label. In comparison, the V17 peak only decreased to 41% of its original intensity at the same waiting time. F23 is less coupled and most likely experiences higher solvent exposure than V17 in the amyloid fibrils, explaining the shorter vibrational lifetime. Overall, these results suggest that secondary structure impacts the lifetime of individual isotope labeled residues, in agreement with previous results on hIAPP,[27] and that the $^{13}C^{18}O$ amide I' modes appear to have inherently longer lifetimes than the sidechain modes that typically interfere with their analysis.

IV. CONCLUSIONS

In this study we have demonstrated that implementing waiting time studies in 2D IR spectroscopy is a powerful approach for differentiating and even suppressing overlapping vibrational modes on the basis of lifetimes. An inherent strength of 2D IR spectroscopy is that it naturally facilitates analysis of modes that are typically not well-defined in pump-probe experiments due to overlapping peaks, crosspeaks, and overtone transitions. Intensity profiles obtained from slices along the 2D IR diagonal fit well to a biexponential function, agreeing with pump-probe experiments. The faster lifetime component, related to dephasing of the vibrational modes, is more prevalent than the slower population relaxation component. As a result, the faster component can be used to differentiate between overlapping features arising from $^{13}C^{18}O$-labeled amide I' modes and various sidechain modes absorbing below 1600 cm^{-1}. We attribute the differences in lifetimes to both differences in solvation and coupling. The unlabeled backbones of MAHP and hIAPP

exhibited the longest lifetimes of all the modes studied, but the 1620 cm^{-1} mode of hIAPP, which arises from highly ordered and strongly coupled β-sheets, is noticeably longer lived at 500 fs than the 375 fs lifetime of the 1650 cm^{-1} mode of MAHP, which arise from primarily disordered structures. Each of the isotope-labeled amide I' modes in MAHP and hIAPP displayed shorter lifetimes than the unlabeled amide I' modes, which we attribute to reduced coupling in those modes when compared to the bulk unlabeled modes. This is supported by the differences in lifetimes for the A5 and A5A8 MAHP isotope labels as the double-labeled A5A8 isotope peak demonstrates a longer lifetime than the single A5 isotope peak even though the local environment is unchanged. Qualitatively, V17 isotope label, which falls within a highly ordered β-sheet of hIAPP, exhibits a smaller decrease in signal intensity than the disordered F23 isotope label at longer waiting times. It was not possible to fit the F23 intensity profile to a biexponential decay due to significant spectral overlap from a crosspeak that grows in between an Arg sidechain and the unlabeled backbone at longer delay times. For a more rigorous quantification of the congested spectral regions, advanced fitting protocols such as lifetime density analysis or the generation of lifetime amplitude spectra could be utilized.[41,42] Regardless, this study has established a waiting time window in which the signal from interfering sidechain modes decays to baseline, but isotope label modes in the same region still have appreciable signal. Therefore, waiting times between ~600-1000 fs can be used to suppress unwanted sidechain signal while still allowing for the identification of backbone and labeled modes. This alleviates the need for point mutations, allowing for the study of native proteins, or for additional isotope labeling to shift sidechain modes into a different spectral window.

SUPPLEMENTARY MATERIALS

Supplementary materials include a table of all fitting parameters, raw pump-probe data for NMA and UL hIAPP, an example of an NMA biexponential fit, hIAPP biexponential fits, and additional 2D IR spectra of UL, A5, and A5A8 MAHP.

ACKNOWLEDGEMENTS

We thank Dr. Kelsey Webb and Ali Fullilove for their preliminary contributions to method development. K.A.H. received stipend support from the National Institutes of Health through the Biophysical Training Program (Grant No. 5T32GM008320-32). This project was supported by startup funding from Vanderbilt University.

AUTHOR DECLARATIONS

Conflict of Interest

The authors have no conflicts to disclose.

Author Contributions

K.H.: Conceptualization (equal); Data curation (lead); Formal analysis (lead); Investigation (lead); Methodology (equal); Validation (lead); Visualization (lead); Writing – original draft (equal). **C.R.:** Data curation (supporting); Formal analysis (supporting); Investigation (supporting); Validation (supporting); Writing – original draft (supporting). **L.B.:** Conceptualization (equal); Formal analysis (supporting); Funding acquisition (lead); Methodology (equal); Project administration (lead); Validation (supporting); Supervision (lead); Writing – original draft (equal).

DATA AVAILABILITY

The data that support the findings of this study are available from the corresponding author upon reasonable request.

REFERENCES

[1] A. Barth, "Infrared spectroscopy of proteins," Biochim Biophys Acta Bioenerg **1767**(9), 1073–1101 (2007).

[2] S. Krimm, and J. Bandekar, "Vibrational spectroscopy and conformation of peptides, polypeptides, and proteins," Adv Protein Chem **38**(C), 181–364 (1986).

[3] L.E. Buchanan, E.B. Dunkelberger, H.Q. Tran, P.-N. Cheng, C.-C. Chiu, P. Cao, D.P. Raleigh, J.J. de Pablo, J.S. Nowick, and M.T. Zanni, "Mechanism of IAPP amyloid fibril formation involves an intermediate with a transient β-sheet," Proceedings of the National Academy of Sciences **110**(48), 19285–19290 (2013).

[4] S.-H.H. Shim, R. Gupta, Y.L. Ling, D.B. Strasfeld, D.P. Raleigh, and M.T. Zanni, "Two-dimensional IR spectroscopy and isotope labeling defines the pathway of amyloid formation with residue-specific resolution," Proceedings of the National Academy of Sciences **106**(16), 6614–6619 (2009).

[5] Y.S. Kim, L. Liu, P.H. Axelsen, and R.M. Hochstrasser, "Two-dimensional infrared spectra of isotopically diluted amyloid fibrils from Aβ40," Proceedings of the National Academy of Sciences **105**(22), 7720–7725 (2008).

[6] C.R. Baiz, M. Reppert, and A. Tokmakoff, in *Ultrafast Infrared Vibrational Spectroscopy*, edited by M.D. Fayer (Taylor & Francis, New York, 2013), pp. 361–403.

[7] K.R. Webb, K.A. Hess, A. Shmidt, K.D. Segner, and L.E. Buchanan, “Probing local changes to α-helical structures with 2D IR spectroscopy and isotope labeling,” Biophys J **122**(8), 1491–1502 (2023).

[8] A. Ghosh, J.S. Ostrander, and M.T. Zanni, “Watching Proteins Wiggle: Mapping Structures with Two-Dimensional Infrared Spectroscopy,” Chem Rev **117**(16), 10726–10759 (2017).

[9] P. Hamm, and M. Zanni, *Concepts and Methods of 2D Infrared Spectroscopy* (Cambridge University Press, Cambridge, 2011).

[10] Y.S. Kim, and R.M. Hochstrasser, “Applications of 2D IR Spectroscopy to Peptides, Proteins, and Hydrogen-Bond Dynamics,” J Phys Chem B **113**(24), 8231–8251 (2009).

[11] W.B. Weeks, C.J. Tainter, and L.E. Buchanan, “Investigating the effects of N-terminal acetylation on KFE8 self-assembly with 2D IR spectroscopy,” Biophys J **121**(8), 1549–1559 (2022).

[12] L.E. Buchanan, M. Maj, E.B. Dunkelberger, P.-N. Cheng, J.S. Nowick, and M.T. Zanni, “Structural Polymorphs Suggest Competing Pathways for the Formation of Amyloid Fibrils That Diverge from a Common Intermediate Species,” Biochemistry **57**(46), 6470–6478 (2018).

[13] C. Fang, J. Wang, Y.S. Kim, A.K. Charnley, W. Barber-Armstrong, A.B. Smith, S.M. Decatur, and R.M. Hochstrasser, “Two-Dimensional Infrared Spectroscopy of Isotopomers of an Alanine Rich α-Helix,” J Phys Chem B **108**(29), 10415–10427 (2004).

[14] C.T. Middleton, A.M. Woys, S.S. Mukherjee, and M.T. Zanni, “Residue-specific structural kinetics of proteins through the union of isotope labeling, mid-IR pulse shaping, and coherent 2D IR spectroscopy,” Methods **52**(1), 12–22 (2010).

[15] K.A. Hess, N.J. Spear, S.A. Vogelsang, J.E. Macdonald, and L.E. Buchanan, “Determining the impact of gold nanoparticles on amyloid aggregation with 2D IR spectroscopy,” Journal of Chemical Physics **158**(9), 91101 (2023).

[16] C. Fang, J. Wang, A.K. Charnley, W. Barber-Armstrong, A.B. Smith, S.M. Decatur, and R.M. Hochstrasser, “Two-dimensional infrared measurements of the coupling between amide modes of an α-helix,” Chem Phys Lett **382**(5–6), 586–592 (2003).

[17] E.H.G. Backus, R. Bloem, P.M. Donaldson, J.A. Ihalainen, R. Pfister, B. Paoli, A. Caflisch, and P. Hamm, “2D-IR Study of a Photoswitchable Isotope-Labeled α-Helix,” J Phys Chem B **114**(10), 3735–3740 (2010).

[18] A. Barth, “The infrared absorption of amino acid side chains,” Prog Biophys Mol Biol **74**(3–5), 141–173 (2000).

[19] A. Ghosh, J. Qiu, W.F. DeGrado, and R.M. Hochstrasser, “Tidal surge in the M2 proton channel, sensed by 2D IR spectroscopy,” Proceedings of the National Academy of Sciences **108**(15), 6115–6120 (2011).

[20] A. Ghosh, J. Wang, Y.S. Moroz, I. V Korendovych, M. Zanni, W.F. Degrado, F. Gai, and R.M. Hochstrasser, “2D IR spectroscopy reveals the role of water in the binding of channel-blocking drugs to the influenza M2 channel,” Journal of Chemical Physics **140**(23), 1–9 (2014).

[21] H. Wu, D.J. Saltzberg, H.T. Kratochvil, H. Jo, A. Sali, and W.F. DeGrado, “Glutamine Side Chain 13C=18O as a Nonperturbative IR Probe of Amyloid Fibril Hydration and Assembly,” J Am Chem Soc **141**(18), 7320–7326 (2019).

[22] R.M. Abaskharon, S.P. Brown, W. Zhang, J. Chen, A.B. Smith, and F. Gai, “Isotope-labeled aspartate sidechain as a non-perturbing infrared probe: Application to investigate the dynamics of a carboxylate buried inside a protein,” Chem Phys Lett **683**, 193–198 (2017).

[23] P. Hamm, M. Lim, and R.M. Hochstrasser, “Structure of the amide I band of peptides measured by femtosecond nonlinear-infrared spectroscopy,” Journal of Physical Chemistry B **102**(31), 6123–6138 (1998).

[24] S. Woutersen, Y. Mu, G. Stock, and P. Hamm, “Subpicosecond conformational dynamics of small peptides probed by two-dimensional vibrational spectroscopy,” Proc Natl Acad Sci U S A **98**(20), 11254–11258 (2001).

[25] K.M. Farrell, N. Yang, and M.T. Zanni, “A polarization scheme that resolves cross-peaks with transient absorption and eliminates diagonal peaks in 2D spectroscopy,” Proc Natl Acad Sci U S A **119**(6), (2022).

[26] L.P. DeFlores, Z. Ganim, S.F. Ackley, H.S. Chung, and A. Tokmakoff, “The anharmonic vibrational potential and relaxation pathways of the amide I and II modes of N-methylacetamide,” Journal of Physical Chemistry B **110**(38), 18973–18980 (2006).

[27] C.T. Middleton, L.E. Buchanan, E.B. Dunkelberger, and M.T. Zanni, “Utilizing lifetimes to suppress random coil features in 2D IR spectra of peptides,” Journal of Physical Chemistry Letters **2**(18), 2357–2361 (2011).

[28] M.F. DeCamp, L. DeFlores, J.M. McCracken, A. Tokmakoff, K. Kwac, and M. Cho, “Amide I vibrational dynamics of N-methylacetamide in polar solvents: The role of electrostatic interactions,” Journal of Physical Chemistry B **109**(21), 11016–11026 (2005).

[29] S.K. Yung, L. Liu, P.H. Axelsen, and R.M. Hochstrasser, “2D IR provides evidence for mobile water molecules in β-amyloid fibrils,” Proc Natl Acad Sci U S A **106**(42), 17751–17756 (2009).

[30] S.Y. Chun, M.K. Son, C.R. Park, C. Lim, H.I. Kim, K. Kwak, and M. Cho, “Direct observation of protein structural transitions through entire amyloid aggregation processes in water using 2D-IR spectroscopy,” Chem Sci **13**(16), 4482–4489 (2022).

[31] S. Hume, G. Hithell, G.M. Greetham, P.M. Donaldson, M. Towrie, A.W. Parker, M.J. Baker, and N.T. Hunt, “Measuring proteins in H2O with 2D-IR spectroscopy,” Chem Sci **10**(26), 6448–6456 (2019).

[32] S. Hume, G.M. Greetham, P.M. Donaldson, M. Towrie, A.W. Parker, M.J. Baker, and N.T. Hunt, "2D-Infrared Spectroscopy of Proteins in Water: Using the Solvent Thermal Response as an Internal Standard," Anal Chem **92**(4), 3463–3469 (2020).

[33] P. Marek, A.M. Woys, K. Sutton, M.T. Zanni, and D.P. Raleigh, "Efficient microwave-assisted synthesis of human islet amyloid polypeptide designed to facilitate the specific incorporation of labeled amino acids," Org Lett **12**(21), 4848–4851 (2010).

[34] B. Błasiak, A.W. Ritchie, L.J. Webb, and M. Cho, "Vibrational solvatochromism of nitrile infrared probes: beyond the vibrational Stark dipole approach," Physical Chemistry Chemical Physics **18**(27), 18094–18111 (2016).

[35] J.Y. Park, S. Mondal, H.J. Kwon, P.K. Sahu, H. Han, K. Kwak, and M. Cho, "Effect of isotope substitution on the Fermi resonance and vibrational lifetime of unnatural amino acids modified with IR probe: A 2D-IR and pump-probe study of 4-azido-L-phenyl alanine," Journal of Chemical Physics **153**(16), 164309 (2020).

[36] D.E. Levin, A.J. Schmitz, S.M. Hines, K.J. Hines, M.J. Tucker, S.H. Brewer, and E.E. Fenlon, "Synthesis and evaluation of the sensitivity and vibrational lifetimes of thiocyanate and selenocyanate infrared reporters," RSC Adv **6**(43), 36231–36237 (2016).

[37] F. Chalyavi, D.G. Hogle, and M.J. Tucker, "Tyrosine as a Non-perturbing Site-Specific Vibrational Reporter for Protein Dynamics," Journal of Physical Chemistry B **121**(26), 6380–6389 (2017).

[38] F. Chalyavi, A.J. Schmitz, N.R. Fetto, M.J. Tucker, S.H. Brewer, and E.E. Fenlon, "Extending the vibrational lifetime of azides with heavy atoms," Physical Chemistry Chemical Physics **22**(32), 18007–18013 (2020).

[39] L.E. Buchanan, E.B. Dunkelberger, and M.T. Zanni, in *Protein Folding and Misfolding*, edited by H. Fabian and D. Naumann (Springer Berlin Heidelberg, Berlin, Heidelberg, 2012), pp. 217–237.

[40] S. Luca, W.M. Yau, R. Leapman, and R. Tycko, "Peptide conformation and supramolecular organization in amylin fibrils: Constraints from solid-state NMR," Biochemistry **46**(47), 13505–13522 (2007).

[41] G.F. Dorlhiac, C. Fare, and J.J. van Thor, "PyLDM - An open source package for lifetime density analysis of time-resolved spectroscopic data," PLoS Comput Biol **13**(5), 1–15 (2017).

[42] S.A. Roget, K.A. Carter-Fenk, and M.D. Fayer, "Water Dynamics and Structure of Highly Concentrated LiCl Solutions Investigated Using Ultrafast Infrared Spectroscopy," J Am Chem Soc **144**(9), 4233–4243 (2022).